ISSN 1027-5495. Functional Materials, 24, No.3 (2017), p. 393-399.
doi:https://doi.org/10.15407/fm24.03.393

$GdVO_4:Eu^{3+}$ nanoparticles — embedded $CaCO_3$ microspheres: synthesis and characterization

***I.I.Bespalova*[1], *S.L.Yefimova*[1], *T.N.Tkacheva*[1], *K.A.Hubenko*, *A.V.Sorokin*[1], *P.V.Mateychenko*[2]**

[1]Institute for Scintillation Materials, STC "Institute for Single Crystals", National Academy of Sciences of Ukraine, 60 Nauky Ave., 61072 Kharkiv, Ukraine
[2]Institute for Single Crystals, STC "Institute for Single Crystals",National Academy of Sciences of Ukraine, 60 Nauky Ave., 61072 Kharkiv, Ukraine

Received March 30, 2017

In present study, we report on synthesis of fluorescent $GdVO_4:Eu^{3+}$ nanoparticle-embedded $CaCO_3$ microparticles ($CaCO_3@GdVO_4:Eu^{3+}$) and their characterization. Synthesized $CaCO_3@GdVO_4:Eu^{3+}$ microspheres are of vaterite polymorph and about 2 μm diameter with −12.80±0.82 mV zeta potential. The specific surface area of the $CaCO_3@GdVO_4:Eu^{3+}$ microspheres and pore size distribution were analyzed by Brunauer-Emmett-Teller method. The microparticles was classified as macroporous ones with a wide distribution of pore sizes.The specific surface area for $CaCO_3@GdVO_4:Eu^{3+}$ microspheres (S_{BET} = 25.2 m^2/g) is higher than reported for $CaCO_3$ microparticles obtained without any additives. $CaCO_3@GdVO_4:Eu^{3+}$ microspheres exhibit strong fluorescence both in a water solution and under fluorescent microscopy conditions that makes them attractive for bio-related application.

Keywords: nanoparticles, microspheres, luminescence, porosity, specific surface area.

Представлен синтез и характеристика микрочастиц $CaCO_3$, содержащих флуоресцентные наночастицы $GdVO_4:Eu^{3+}$ ($CaCO_3@GdVO_4:Eu^{3+}$). Синтезированные микросферы $CaCO_3@GdVO_4:Eu^{3+}$ полиморфной модификации ватерит имеют диаметр порядка 2 мкм с дзета-потенциалом −12,80±0,82 мВ. Удельная площадь поверхности микросфер $CaCO_3@GdVO_4:Eu^{3+}$ и распределение пор по размерам проанализированы методом Брунауэра-Эммета-Теллера, что позволило отнести их к макропористым частицам с широким распределением пор по размерам. Удельная площадь поверхности $CaCO_3@GdVO_4:Eu^{3+}$ ($S_{уд}$ = 25,2 м^2/г) выше, чем микрочастиц $CaCO_3$, полученных без каких-либо добавок. Микрочастицы $CaCO_3@GdVO_4:Eu^{3+}$ обладают интенсивной флуоресценцией при УФ возбуждении как в водном растворе, так и в условиях флуоресцентной микроскопии, что делает их привлекательными для биологического применения.

Мікросфери $CaCO_3@GdVO_4:Eu^{3+}$: синтез та характеризація. *І.І.Беспалова, С.Л.Єфімова, Т.М.Ткачова, К.О.Губенко, А.В.Сорокін, П.В.Матейченко.*

Представлено синтез і характеристика мікрочастинок $CaCO_3$, що містять флуоресцентні наночастинки $GdVO_4:Eu^{3+}$ ($CaCO_3@GdVO_4:Eu^{3+}$). Синтезовані мікросфери $CaCO_3@GdVO_4:Eu^{3+}$ поліморфної модифікації ватерит мають діаметр близько 2 мкм з дзета-потенціалом −12,80±0,82 мВ. Питома площа поверхні мікросфер $CaCO_3@GdVO_4:Eu^{3+}$ і розподіл пор за розмірами проаналізовано методом Брунауера-Еммета-Теллера, що дозволило віднести їх до макропористих частинок з широким розподілом пор за розмірами. Питома площа поверхні $CaCO_3@GdVO_4:Eu^{3+}$ ($S_{пт}$= 25,2 м^2/г) вище, ніж мікрочастинок $CaCO_3$, отриманих без будь-яких добавок. Мікрочастинки $CaCO_3@GdVO_4:Eu^{3+}$ мають інтенсивну флуоресценцію при УФ випроміненні як у водному розчині, так і в умовах флуоресцентної мікроскопії, що робить їх привабливими для біологічного застосування.

1. Introduction

Recently, a wide range of studies has been focused on the development of micro- and nano-scale materials for biomedical purposes. Variety of micro- and nanoparticles (lipid, polymeric, inorganic and hybrid) were synthesized for targeted drug and growth factor delivering [1–4], gene therapy [3], tissue engineering [4, 5], medical imaging [6, 7], etc. Many advantages of nano-particle drug delivery has been reported [1, 8]. Delivering of drug via nanoparticles allows tissue- and cell-specific drug delivering, reducing collateral damage to healthy tissues, improves the solubility of poorly water-soluble drugs, prolongs the half-life of its systemic circulation. Such carriers can ensure drug release at a sustained rate or in an stimuli-responsive manner [1, 8]. However, in certain applications such as *in vivo* micro-chip [10], local drug-delivery strategy [10], and tumor targeting and body fluid analysis [11, 12] a carries uptake by cells is not required or even undesirable. For these purposes, micro-scale particles, including porous ones with the same advantages could be used [4, 12–17].

Theranostics, which integrate both therapeutic and diagnostic capabilities into a single platform, is a new pioneering approach in modern biomedical researches [18]. This approach allows combination of both therapeutic (drugs) and diagnostic or other agents (fluorescent molecules or nanoparticles, iron oxide nanoparticles, etc.) in a novel therapeutic formulation. Micro-scale particles encapsulated fluorescent agents and drugs have been designed for drug delivery to the joint and other tissues [13, 19] cancer therapy [17, 20], bacteria elimination [21].

Porous microparticles, in particular, porous calcium carbonate microspheres $CaCO_3$, are of special interest for theranostic applications due to their advantages such as high specific surface area, large pore volume, biocompatibility [22–24]. $CaCO_3$ microspheres were considered as vehicles for drug delivery *in vitro* and *in vivo* experiments for the encapsulation of such drugs as insulin, anticancer drug doxorubicin hydrochloride, and ibuprofen and provided their sustained release in the site of action [24–31]. Such micro vehicles could be also loaded with fluorescent agents (fluorescent dye molecules, quantum dots or rare-earth based nanoparticles) that will allow visualization and monitoring of their accumulation inside the body or tissues.

In the present study, we report the synthesis of porous vaterite calcium carbonate microparticles loaded with europium-doped gadolinium orthovanadate nanoparticles ($GdVO_4$:Eu^{3+}) and their characterization (SEM, TEM images, specific surface area, pore size and volume, FTIR spectra and optical characteristics). Optical properties and low cytotoxicity of rare-earth doped nanoparticles (NPs) make them promising for biomedical applications [32, 33]. Attractive properties of rare-earth doped NPs include high photostability, absence of blinking effect, extremely narrow emission bands with a large Stokes shifts, long lifetimes [32, 33]. Moreover, the high magnetic moment of such ions as Gd^{3+}, under magnetic field renders them potent contrast agents for magnetic resonance imaging. Thus, porous $CaCO_3$ vehicles "labeled" with $GdVO_4$:Eu^{3+} NPs could be visualized by both fluorescent and magnetic resonance imaging.

2. Materials and methods

2.1. Materials

Gadolinium chlorides (99.9 %), disodium EDTA·2Na (99.8 %) and anhydrous sodium metavanadate ($NaVO_3$, 96 %) were obtained from Acros organic (USA) and all used without further purication. Sodium hydroxide (99 %) was purchased from Macrohim (Ukraine). Sodium orthovanadate Na_3VO_4 solution was obtained by adding a 1M solution of NaOH in aqueous solution $NaVO_3$ to pH = 13. Anionic polyelectrolyte poly(sodium 4-styrenesulfonate) (PSS, average $Mw \approx 70\ 000$ g/mol, powder) were purchased from Sigma-Aldrich (USA) and used as received. Calcium chloride ($CaCl_2$, Khimlabreaktiv, Ukraine) and sodium carbonate (Na_2CO_3, Khimlabreaktiv, Ukraine) were analytical reagents and used as received.

2.2. $GdVO_4$:Eu^{3+} NPs synthesis

Aqueous colloidal solutions of gadolinium orthovanadate nanoparticles doped with europium ions $Gd_{0.9}Eu_{0.1}VO_4$ ($GdVO_4$:Eu^{3+}) were synthesized according to the method reported earlier [34]. Synthesized NPs were characterized using Transmission Electron Microscopy (TEM-125K electron microscope, Selmi, Ukraine), X-ray diffraction analysis (Siemens D500 X-ray diffractometer, Germany) and Dynamic Light Scattering method (ZetaPALS analyzer, Brookhaven Instruments Corp., USA). The concentration of $GdVO_4$:Eu^{3+} NPs in a water colloidal solution was 1 g/l.

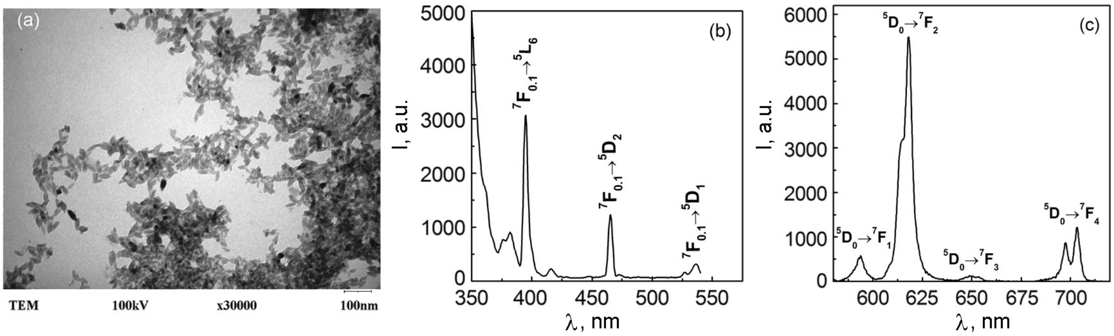

Fig. 1. TEM image (a), excitation, λ_{reg} = 618 nm (b) and emission, λ_{exc} = 280 nm (c) spectra of $GdVO_4:Eu^{3+}$ nanoparticles.

2.3. Synthesis of spherical vaterite $CaCO_3$ and $GdVO_4:Eu^{3+}$ — doped $CaCO_3$ microspheres ($CaCO_3@GdVO_4:Eu^{3+}$)

Spherical $CaCO_3$ microparticles were obtained by the method based on rapid mixing of equal volume of aqueous solutions containing Ca^{2+} and CO_3^{2-} ions [22, 24]. To prepare vaterite polymorphic modification of $CaCO_3$, we used a structure-forming agent poly(sodium 4-styrenesulfonate), PSS. First, 0.08 g PSS was equally dissolved in a $CaCl_2$ solution (10 ml, 0.3 M) and in a Na_2CO_3 solution (10 ml, 0.3 M). The final PSS concentration was 4 mg/ml. Then the obtained solutions were rapidly poured together and the mixture was vigorously stirred during 45 min at 23–24°C. The precipitated PSS-doped $CaCO_3$ microparticles were centrifuged at 2500 rpm for 3 min (Centrifuge Multi-spin MSC-6000, Biosan, Latvia), washed three times by pure water, and dried in air at 60°C.

For synthesis of $CaCO_3@GdVO_4:Eu^{3+}$ microspheres, 0.5 ml of an aqueous solution of $GdVO_4:Eu^{3+}$ NPs (1 g/l) was added into 9.5 ml of $CaCl_2$ solution (0.3 M) containing PSS. Then, the synthesis procedure was the same as for PSS-doped $CaCO_3$ microparticles.

2.4. Instrumentation and characterization

Synthesized PSS-doped $CaCO_3$ and $CaCO_3@GdVO_4:Eu^{3+}$ microparticles were characterized by scanning electron microscopy (SEM, JSM-6390LV, (JEOL Company, USA)) operated at 15 kV and transmission electron microscopy (TEM, JEM-2100F (JEOL Company, Japan)) operated at 200 kV, equipped with an Oxford CCD camera. FT-IR spectra were recorded with a Perkin-Elmer Spectrum One B FT-IR spectrometer (USA) in the range of 4000–400 cm^{-1} using KBr pellets. The specific surface area, porous volume, and porous size distribution of PSS-doped $CaCO_3$ and $CaCO_3@GdVO_4:Eu^{3+}$ microparticles were determined using a Surface Area and Porosimetry System JW-BK132F (Beijing TWGB Sci. & Tech. Co., Ltd, China). Zeta-potential of synthesized NP_S and microparticles were measured with a ZetaPALS analyzer (Brookhaven Instruments Corp., USA) operated in phase analysis light scattering mode.

Fluorescence and fluorescence excitation spectra were taken with a Lumina spectrofluorimeter (Thermo Scientific, USA). Fluorescence images of $CaCO_3@GdVO_4:Eu^{3+}$ microspheres were taken using a confocal laser scanning microscope ZeissLSM510 Meta (Germany) with a 20× objective lens. The luminescence was excited using a diode laser 405 nm, 25 mW and collected using BP 604-625 filter for Eu^{3+} luminescence detection.

3. Results and discussion

TEM image of synthesized $GdVO_4:Eu^{3+}$ nanoparticles is presented in Fig. 1a and reveals well-crystallized spindle-like particles of 10×30 nm ±5 nm size. To stabilize $GdVO_4:Eu^{3+}$ nanoparticles in aqueous solutions, disodium EDTA·2Na was used during the synthesis, which carboxylate groups impart a negative charge to the nanoparticle surface. The overage hydrodynamic diameter of $GdVO_4:Eu^{3+}$ nanoparticles is 47±1.5 nm, zeta-potential is −22.03±2.2 mV. XRD pattern of synthesized $GdVO_4:Eu^{3+}$ nanoparticlesis presented in Fig. 2a and shows (200), (112), and (312) reflections, which are typical for tetragonal phase of the zircon type [35, 36].

The luminescence excitation and emission spectra of synthesized $GdVO_4:Eu^{3+}$ nanoparticles are shown in Fig. 1,b,c. The excitation spectrum corresponding to the Eu^{3+} emission (Fig. 1b) consists of the intense wide band with the maximum about 280 nm

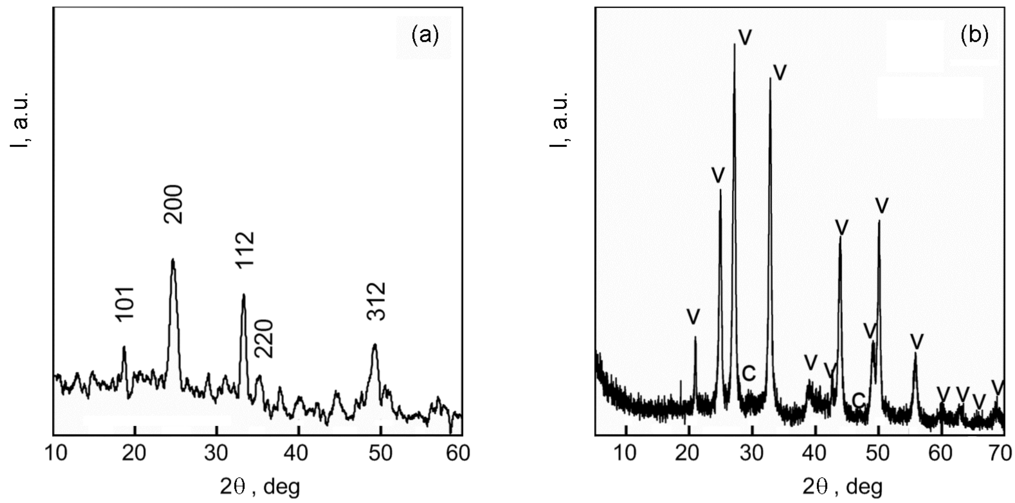

Fig. 2. XRD patterns of $GdVO_4$:Eu^{3+} nanoparticles (a) and $CaCO_3$ microspheres (b).

(a charge transfer from oxygen vacancies to the vanadate groups VO_4^{3-}) and several weaker bands in the longer-wavelength region (the $f \rightarrow f$ transitions of europium ions within the $4f^6$ electron configuration) [37, 38]. The luminescence spectrum of $GdVO_4$:Eu^{3+} nanoparticles (Fig. 1c) results from transition within the f-electron configuration of the europium ions. The main contribution is the $^5D_0$–$^7F_{2,4}$ forced electric-dipole transitions, whereas other components of weaker importance are the $^5D_0$–$^7F_{1,3}$ magnetic dipole transitions [38].

It is known that calcium carbonate occurs in three anhydrous polymorphic forms: calcite, aragonite, and vaterite [22–24, 26]. The vaterite polymorph owing to its spherical morphology and porous surface is the most attractive phase of $CaCO_3$ for bio-related applications. Being inert, micro/nanosized and porous, it has the ability to be loaded with various compounds and hence act as tremendous vehicles for drugs, proteins and enzymes [22–24, 26]. However, vaterite easily undergoes the phase transition to the more thermodynamically stable phase of $CaCO_3$, calcite, which occurs within several hours for vaterite samples kept in aqueous solution [22, 23, 26]. So, many efforts were made to obtain stable porous vaterite polymorph. To stabilize vaterite form, various dispersants and structure-forming agents were used, such as polymer molecules, anionic starburst dendrimer, nanoparticles, polypeptides and other molecules [22–24]. In our previous work, we reported on synthesis stable vaterite spheroids using a negatively charged polyelectrolyte PSS as a dispersant and structure-forming agent [39]. In this study, we also use NPs that could affect the structure and porosity of the obtained $CaCO_3$ microspheres. Fig. 3 represent SEM and TEM images of synthesized PSS-doped $CaCO_3$ microspheres and those synthesized with both PSS and $GdVO_4$:Eu^{3+} NPs ($CaCO_3$@$GdVO_4$:Eu^{3+}). Both images show typical structure of polycrystalline spheroids, without other polymorphs, which are often observed in samples synthesized without additives [24, 39]. XRD pattern of the $CaCO_3$ microparticles exhibits the characteristic reflections of vaterite phase (Fig. 2b). The microspheres reveal some size distribution with the mean diameter of 2.18±0.44 μm and 1.92±0.43 μm for $CaCO_3$ and $CaCO_3$@$GdVO_4$:Eu^{3+} microparticles, respectively. So, NPs embedding into $CaCO_3$ does not provoke increase or remarkable decrease of the microsphere's size. In case of PSS-doped $CaCO_3$ microspheres, the TEM image (Fig. 3b) clear shows that spheroids are composed of smaller single crystal subunits (framboid or raspberry), which are typical for vaterite polymorph [23, 39, 40]. In case of $CaCO_3$@$GdVO_4$:Eu^{3+} microparticles, such a framboid structure is not so pronounced, due to $GdVO_4$:Eu^{3+} NPs embedded into the microspheres (Fig. 3d). Measured zeta-potential of the microspheres is −13.87±0.82 mV for $CaCO_3$ and −12.80±0.82 mV for $CaCO_3$@$GdVO_4$:Eu^{3+}. The negative charge is governed by the PSS anions used for vaterite polymorph stabilization.

FT-IR spectra of $CaCO_3$ and $CaCO_3$@$GdVO_4$:Eu^{3+} microspheres (Fig. 4) reveal the number of fundamental bands centered at 1498, 1089, 878, 746 cm^{-1} which are attributed to the four normal vi-

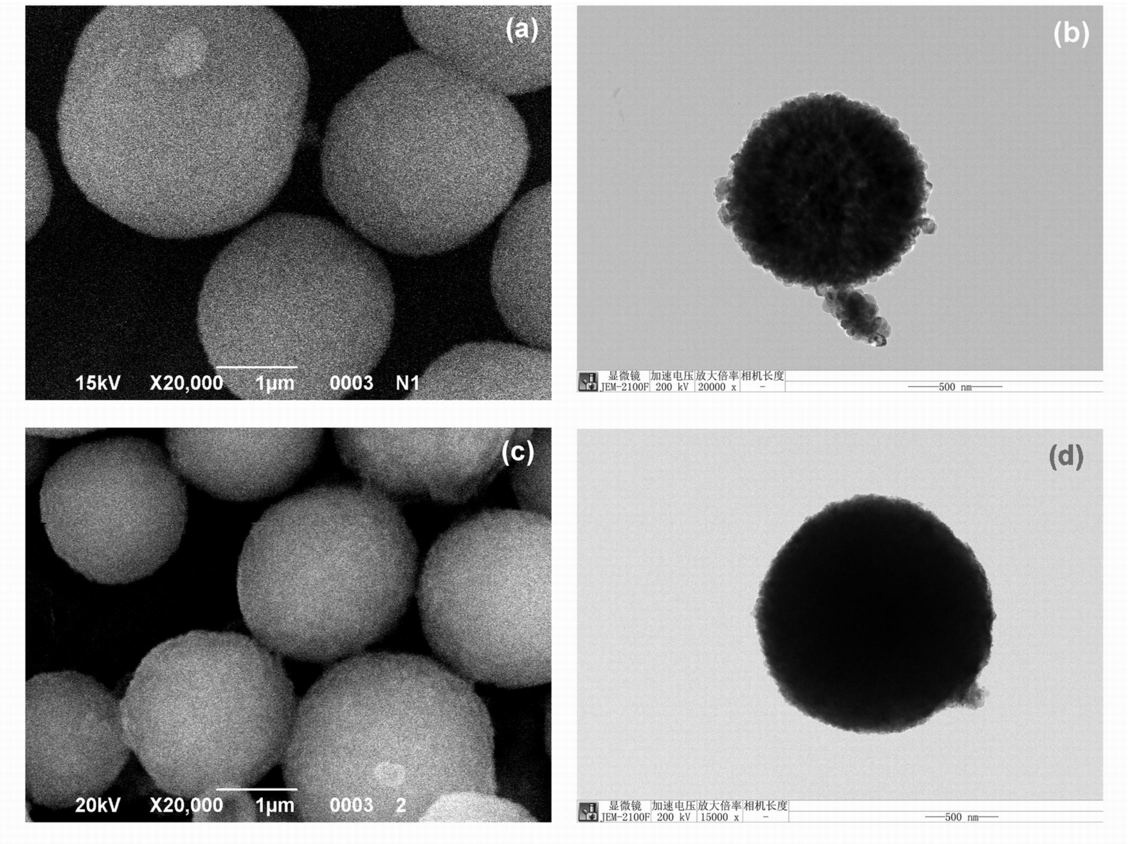

Fig. 3. SEM (a, c) and TEM (b, d) images of PSS-doped $CaCO_3$ (a, b) and $CaCO_3$@$GdVO_4$:Eu^{3+} (c, d) microspheres.

brations of ions in vaterite polymorph [41–43]. The bands centered near 1175, 1127, 1046, 1011 and 836 cm^{-1} belong to PSS vibrations [44, 45]. For $CaCO_3$@$GdVO_4$:Eu^{3+} microspheres (Fig. 4, curve 2), the peak located at 833 cm^{-1}, which is related to a symmetric stretching vibration along V–O–V bonds [46, 47] and two peaks at 1396 cm^{-1} and 1570 cm^{-1} attributed to the symmetrical and asymmetrical valence vibrations of the carboxylate groups O-C=O in disodium EDTA·2Na were not observed [48]. Probably, it could be explained by the relatively small concentration of $GdVO_4$:Eu^{3+} nanoparticles stabilized by EDTA and overlapping of the vibration V–O–V band with the PSS band centered at 836 cm^{-1} and the vibration bands of carboxylate with very strong band at 1498 cm^{-1} (Fig. 4).

The N_2 adsorption/desorption isotherm for $CaCO_3$ and $CaCO_3$@$GdVO_4$:Eu^{3+} microspheres are shown in Fig. 5. The nitrogen adsorption isotherm for $CaCO_3$ microspheres could be classified as type-IV with H3 hysteresis loop according to Brunauer-Deming-Deming-Teller (BDDT) classfication that indicates materials containing of both mesopores and micropores of bottle-shape

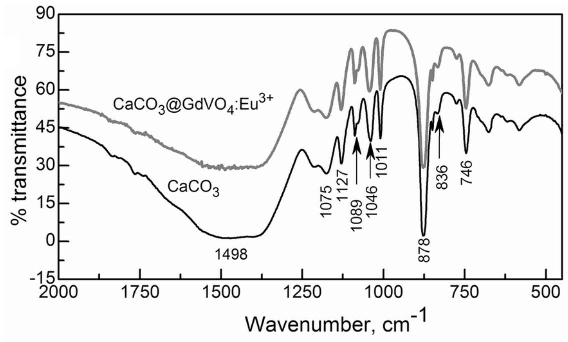

Fig. 4. FT-IR spectra of PSS-doped $CaCO_3$ and $CaCO_3$@$GdVO_4$:Eu^{3+} microspheres.

structures (wide openings and narrow "necks") or slit-type (Fig. 5a) [49, 50]. Since capillary condensation for $CaCO_3$@PSS microspheres starts at P/P_0, the pores could be mainly composed of mesopores with the average pore diameter of 6.7 nm estimated using the Barrett-Joyner-Halenda (BJH) method from the desorption branch of the isotherm [49]. The specific surface qarea of $CaCO_3$ microspheres $S_{BET} = 51.6$ m^2/g was calculated using the Brunauer-Emmet-Teller (BET) method. The nitrogen adsorption isotherm for $CaCO_3$@$GdVO_4$:Eu^{3+} microspheres could

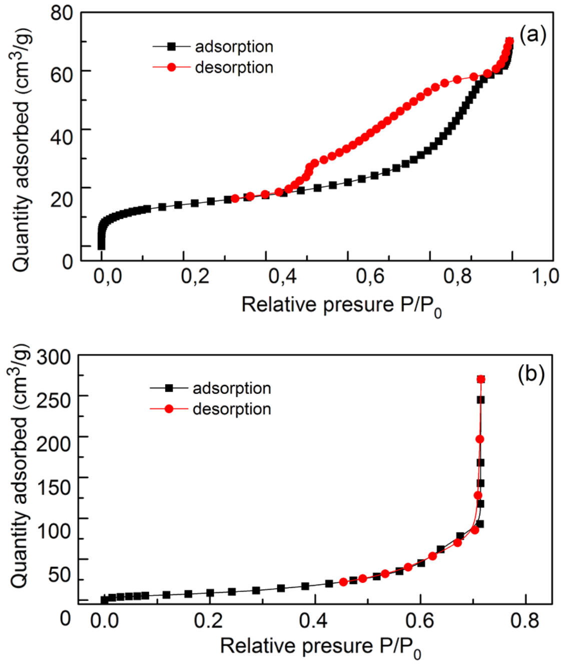

Fig. 5. N_2 adsorption/desorption isotherms for PSS-doped $CaCO_3$ (a) and $CaCO_3$@$GdVO_4$:Eu^{3+} (b) microspheres.

be classified as type-II (Fig. 5b) indicating macroporous materials with a wide distribution of pore sizes and strong adsorbent/adsorbate interaction, which is also confirmed by the BET constant value $C = 57.16$ [49, 50].The point of flexion, which indicates the completion of monolayer formation, is observed at the low relative pressure value, and then the indefinite multi-layer formation without saturation limit occurs. The calculated specific surface area for $CaCO_3$@$GdVO_4$:Eu^{3+} microspheres S_{BET} = 25.2 m^2/g. Since capillary condensation is not characteristic for macroporous materials, the BJH method is not applicable for the estimation of pore volume and pore size distribution. The obtained values for both types of microspheres are much higher than that of $CaCO_3$ microparticles obtained without additives (3.2–8.8 m^2/g) [22, 23].

Fig. 6 represents the fluorescence spectrum obtained from water solution containing $CaCO_3$@$GdVO_4$:Eu^{3+} microspheres (a) and its fluorescence image (b). Despite the relatively small concentration of the $GdVO_4$:Eu^{3+} nanoparticles entrapped in $CaCO_3$ microspheres, the fluorescence spectrum clear demonstrates the spectral lines typical for Eu^{3+} luminescence in the vanadate matrix (see Fig. 1c). We also observe fluorescence of $CaCO_3$@$GdVO_4$:Eu^{3+} microspheres governed by Eu^{3+} ions under laser excitation in a fluorescence microscope.

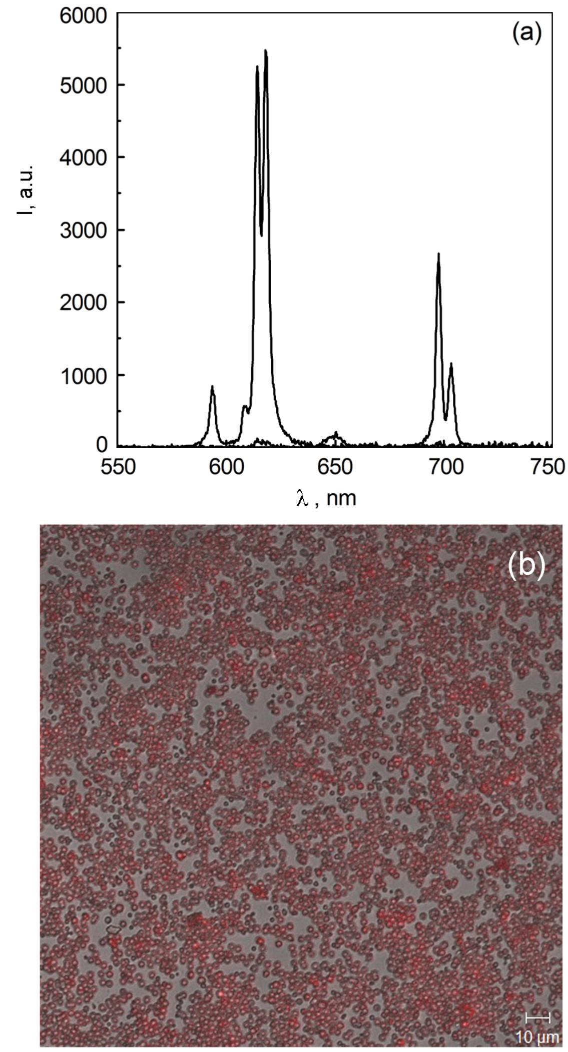

Fig. 6. Fluorescence spectrum of aqueous solution containing $CaCO_3$@$GdVO_4$:Eu^{3+} microspheres, λ_{exc} = 280 nm (a) and fluorescence image of $CaCO_3$@$GdVO_4$:Eu^{3+} microspheres, λ_{exc} = 405 nm (b).

4. Conclusions

Porous vaterite calcium carbonate microspheres loaded with europium-doped gadolinium orthovanadate nanoparticles $CaCO_3$@$GdVO_4$:Eu^{3+} were synthesized and compared with those obtained without $GdVO_4$:Eu^{3+} NPs. It has been revealed that the embedding of $GdVO_4$:Eu^{3+} NPs does not affect the size of $CaCO_3$@$GdVO_4$:Eu^{3+} microspheres (d = 1.92±0.43 μm), where as changes its porosity. The N_2 adsorption/desorption isotherm for $CaCO_3$@$GdVO_4$:Eu^{3+} indicates that the microparticles contains macropores with a wide distribution of pore sizes. The specific surface area for $CaCO_3$@$GdVO_4$:Eu^{3+} microspheres (S_{BET} = 25.2 m^2/g) is smaller than that for PSS-doped $CaCO_3$

(S_{BET} = 51.6 m^2/g), but higher than S_{BET} reported for $CaCO_3$ microparticles obtained without additives. The aqueous solution of $CaCO_3$@$GdVO_4$:Eu^{3+} microspheres were stable during long time period without vaterite polymorph modification to more stable calcite, $CaCO_3$@$GdVO_4$:Eu^{3+} microparticles exhibit strong fluorescence in a solution and under fluorescent microscopy conditions. Synthesized $CaCO_3$@$GdVO_4$:Eu^{3+} microparticles are attractive for theranostic applications.

Acknowledgments. The authors thank to Prof. Xiaoqiang Cui (School of Material Science and Engineering, Jilin University, China) for his assistance with TEM images. This work was supported by National Academy of Sciences of Ukraine (Project No. 0116U002612). The authors declare that they have no conflict of interest.

References

1. D.Liu, F.Yang, F.Xiong et al., *Theranostics*, **6**, 1306 (2016).
2. K.Kim, D.Pack, *BioMEMS Biomed Nanotechn*, **1**, 19 (2015).
3. J.Panyam, V.Labhasetwar, *Adv. Drug Delivery Rev.*, **55**, 329 (2003).
4. N.P.Omorphos, L.Kahn, D.M.Kalaskar, *Colloids and Surf. B: Biointerfaces*, **136**, 440 (2015).
5. P.Newman, A.Minett, R.Ellis-Behnke et al., *Nanomedicine*, **9**, 1139 (2013).
6. H.M.Hertz, J.C.Larsson, U.Lundstrom et al., *Opt. Lett.*, **39**, 2790 (2014).
7. C.Sun, J.S.H. Lee, M.Zhang, *Adv. Drug Delivery Rev.*, **60**, 1252 (2008).
8. L.Zhang, F.X.Gu, J.M.Chan et al., *Clinical Pharmacology & Therapeutics*, **83**, 761 (2008).
9. A.Zaccaria, A.Bouamrani, L.Selek et al., *ACS Chem. Neurosci.*, **4**, 385 (2013).
10. J.B.Wolinsky, Y.L.Colson, M.W.Grinstaff, *J. Control. Release*, **159**, 14 (2012).
11. W.Qin, K.Li, G.Feng et al., *Adv. Funct. Mater.*, **24**, 635 (2014).
12. C.-L.Sun, T.Li, J.-Q.Jiang et al., *J. Mater. Chem. B*, 4, 7226 (2016).
13. N.Butoescu, Ch.A.Seemayer, G.Palmer et al., *Arthritis Research & Theraphy*, **11**, R72 (2009).
14. S.Haruta, T.Hanafusa, H.Fukase et al., *DiabetesTech. Ther.*, **5**, 1 (2003).
15. M.Higaki, M.Kameyama, M.Udagawa et al., *Diabetes Tech. Ther.*, **8**, 369 (2006).
16. W.Yang, D.Trau, R.Renneberg et al., *J. Coll. Interface Sci.*, **234**, 356 (2001).
17. T.Patino, J.Soriano, L.Barrios et al., *Sci. Rep.*, **5**, 11371 (2015).
18. J.Wang, H.Cui, *Theranostics*, **6**, 1274 (2016).
19. Y.Geng, P.Dalhaimer, S.Cai et al., *Nat. Nanotechnol.*, **2**, 249 (2007).
20. K.Y.Win, E.Ye, C.P.Teng et al., *Adv. Healthcare Mater.*, **2**, 1571 (2013).
21. M.Behra, N.Azzouz, S.Schmidt et al., *Biomacromolecules*, **14**, 1927 (2013).
22. D.Volodkin, *Adv. Colloid Interf. Sci.*, **207**, 306 (2014).
23. D.B.Trushina, T.V.Bukreeva, M.V.Kovalchuk et al., *Mater. Sci. Engin. C*, **45**, 644 (2014).
24. Y.Boyjoo, V.K.Pareek, J.Liu, *J. Mat. Chem. A*, **2**, 14270 (2014).
25. Y.Ueno, H.Futagawa, Y.Takagi et al., *J. Control. Release*, **103**, 93 (2005).
26. D.V.Volodkin, N.I.Larionova, G.B.Sukhorukov, *Biomacromolecules*, **5**, 1962 (2004).
27. C.Peng, Q.Zhao, C.Gao, *Colloid Surface A*, **353**, 132 (2010).
28. C.Wang, C.He, Z.Tong et al., *Int. J. Pharm.*, **308**, 160 (2006).
29. S.Haruta, T.Hanafusa, H.Fukase et al., *DiabetesTech. Ther.*, **5**, 1 (2003).
30. M.Higaki, M.Kameyama, M.Udagawa et al., *DiabetesTech. Ther.*, **8**, 369 (2006).
31. J.Wang, J.-S.Chen, J.-Y.Zong et al., *J. Phys. Chem. C*, **114**, 18940 (2010).
32. C.Bouzigues, T.Gacoin, A.Alexandrou, *Acs Nano*, **11**, 8488 (2011).
33. J.Shen, L.-D.Sun, C.-H.Yan, *Dalton. Trans.*, **14**, 5687 (2008).
34. V.K.Klochkov, A.I.Malyshenko, O.O.Sedyh et al., *Functional Materials*, **1**, 111 (2011).
35. B.C.Chakoumakos, M.M.Abraham, L.A.Boatner, *J. Solid State Chem.*, **109**, 197 (1994).
36. J.A.Baglio, G.Gashurov, *Acta Cryst. B*, **24**, 292(1968).
37. C.Hsu, R.C.Powell, *J. Luminescence*, **10**, 273 (1975).
38. A.Huignard, V.Buissette, A.C.Franville et al., *J. Phys. Chem. B*, **107**, 6754 (2003).
39. S.Ouhenia, D.Chateigner, M.A.Belkhir et al., *J. Cryst. Growth*, **310**, 2832 (2008).
40. N.A.N.Hanafy, M.L.De Giorgi, C.Nobile et al., *J. Basic Appl. Sci.*, **4**, 60 (2015).
41. F.A.Andersen, L.Brecevic, *Acta Chem. Scand.*, **45**, 1018 (1991).
42. J.Chen, L.Xiang, *Powder Technol.*, **189**, 64 (2009).
43. H.Nebel, M.Neumann, C.Mayer, *Matthias Epple, Inorg. Chem.*, **47**, 7874 (2008).
44. C.Du, J.Shi, L.Zhang et al., *Mater. Sci. Eng. C*, **33**, 3745 (2013).
45. A.Bragaru, M.Kusko, A.Radoi, *Cent. Eur. J. Chem.*, **11**, 205 (2013).
46. J.Tang, A.P.Alivistatos, *Nano Lett.*, **6**, 2701 (2006).
47. D.K.Kanchan, H.R.Panchal, *Turk. J. Phys.*, **22**, 989 (1998).
48. D.Lin-Vien, N.Colthup, W.Fateley et al., The Handbook of IR and Raman Characteristic Frequencies of Organic Molecules, Academic Press, New York (1991).
49. J.B.Condon, Surface Area and Porosity Determinations by Physisorption: Measurement and Theory, Elsevier, Amsterdam (2006).
50. S.J.Cregg, K.S.W.Sing, Adsorption, Surface Area and Porosity, Academic Press, London, New York (1967).